Journal of Industrial and Engineering Chemistry 26 (2015) 173–181

Contents lists available at ScienceDirect

Journal of Industrial and Engineering Chemistry

journal homepage: www.elsevier.com/locate/jiec

A facile method for enhancing photovoltaic performance of low-band-gap D–A conjugated polymer for OPVs by controlling the chemical structure

Min Hee Choi, Kwan Wook Song, Soo Won Heo, Yong Woon Han, Doo Kyung Moon *

Department of Materials Chemistry and Engineering, Konkuk University, 1 Hwayang-dong, Gwangjin-gu, Seoul 143-701, Republic of Korea

ARTICLE INFO

Article history:
Received 8 August 2014
Received in revised form 21 October 2014
Accepted 28 October 2014
Available online 4 December 2014

Keywords:
Thiophene
Thienothiophene
Benzothiadiazole
Stille coupling reaction
Bulk heterojunction polymer solar cells

ABSTRACT

Stille coupling polymerization has been used to synthesize a series of new crystalline conjugated polymers with low-lying HOMO level: PABToBT, PPDToBT, PQTDPT. All of these polymers exhibited sufficient energy offsets with respect to those of fullerenes to allow efficient charge transfer and low-lying highest occupied molecular orbital (HOMO), from −5.04 to −5.27 eV. As a result, the photovoltaic device comprising a PPDToBT/$PC_{71}BM$ (1:4) blend system exhibited excellent performance, under AM1.5 G irradiation, with a V_{OC} of 0.878 V, a J_{SC} of 8.7 mA cm^{-2}, a FF of 0.51, and a promising PCE of 3.9%.

Introduction

For the past several decades, aromatic ring-based conjugated polymers have been applied in the fabrication of various electronic devices, such as organic light-emitting diodes (OLEDs) [1–4], organic thin-film transistors (OTFTs) [5–7], and organic photovoltaic cells (OPVs) [8–12]. In particular, polymer solar cells (PSCs) with a bulk heterojunction (BHJ) structure in which a π-conjugated polymer donor and soluble fullerene derivative acceptors are combined have recently attracted a much attention due to advantages such as low cost, light weight, and flexibility [13–15].

Regio-regular poly(3-hexylthiophene) (P3HT) is a leading polymer donor for use in PSCs, whereas [6,6]-phenyl-C61-butyric acid methyl ester (PCBM) is the most widely used acceptor. P3HT/PCBM-based devices with a power conversion efficiency (PCE) of up to 4–5% have been reported [16,17]. The PCE of the P3HT/PCBM system does not increase any further for the following reasons. First, the relatively large band gap (1.9 eV) of P3HT disturbs the effective light harvesting of photovoltaics [18,19]. Second, the low energy difference of the lowest unoccupied molecular orbital (LUMO) and highest occupied molecular orbital (HOMO) levels causes P3HT/PCBM-based PSCs to have a low open-circuit voltage (V_{OC}, ~0.6 V) [20]. Recently, there has been demand for a polymer photovoltaic donor material with a low band gap and low HOMO energy level to facilitate the improvement of PSC efficiency [21–26]. Because the V_{OC} is determined by the difference between the HOMO (donor) and LUMO (acceptor) levels, it is a key factor in reducing the HOMO level of a donor polymer. A donor polymer with a low HOMO energy level not only allows for a higher V_{OC} but also results in high oxidative stability. Moreover, because durability is of great concern for industrial applications, the stability of materials in the field of organic electronics is regarded as an important property of organic semiconductors [27].

The synthesis of conjugated polymers intended to fabricate a polymer solar cell device with a high light-harvesting ability (low band gap) and open-circuit voltage is still dependent on the concept of donor–acceptor (D–A) alternate copolymers [28] because an electron donor unit can provide a low HOMO level and an electron acceptor unit can regulate the electronic band gap of a polymer. Several studies have reported using this approach on benzothiadiazole and various alkyl thiophene unit-based copolymers [29,30]. Among the derivatives with a low HOMO energy level, fused thiophene rings have a higher resonance stabilization energy than single thiophene molecules, which in turn reduces the HOMO energy level of the resulting copolymer [31,32]. In the polythiophene derivatives in which fused thiophene is introduced into the backbone, high molecular ordering characteristics and

* Corresponding author. Tel.: +82 2 450 3498; fax: +82 2 444 0765.
E-mail address: dkmoon@konkuk.ac.kr (D.K. Moon).

http://dx.doi.org/10.1016/j.jiec.2014.10.045
1226-086X/

high charge-carrier mobility have also been observed due to the planarity and rotational invariance of the thienothiophene unit [33]. As a way to obtain a larger absorption region by decreasing the band gap, the acceptor unit responsible for the electron-withdrawing properties of a copolymer could be introduced to the main chain of the polymer to yield a D–A-type polymer. 2,1,3-Benzothiadiazole (BT) and di-2-thienyl-2,1,3-benzothiadiazole (DTBT) are known as common strong electron acceptors. Recently, many studies have been published on how to improve the characteristics of OPVs by introducing DTBT. However, DTBT has a strong stacking ability due to its constituent thiophene units. As a result, synthesized polymers have low solubility and low molecular weight.

Heiser et al. reported the synthesis of a PTBzT-series polymer using thienothiophene and DTBT. Even though an attempt was made to increase the solubility and the degree of polymerization of the polymer via the introduction of a dodecyl chain to the thiophene spacer, the molecular weight (M_n, the number average molecular weight) and V_{OC} were as low as 12,000–16,000 and 0.55–0.67 V, respectively [34]. Since this time, the HOMO level has been reduced to as low as −5.43 eV by increasing the number of dodecyl thiophene units in the molecular structure. In contrast, the V_{OC} has remained at 0.79 V. With a decrease in FF after a morphology decline, PCE remained at 1.8% [28]. Therefore, studies have been reported in which the molecular weight increased when using DTBT derivatives with a side chain introduced; such polymers have been observed to exhibit good solubility [35–42]. A previous study reported results on the use of thienothiophene derivatives as a donor and quinoxaline derivatives with high solubility instead of DTBT as an acceptor. When pentadecyl thienothiophene instead of thienothiophene was introduced, a very low HOMO level was observed (−5.6 eV). Due to the steric hindrance and tilt caused by a long and bulky pentadecyl chain, however, low polymerization and a large band gap were found. PQTPDTT, to which a thiophene spacer was introduced, showed a relatively high V_{OC} (0.71 V) and low band gap (1.7 eV), and the best PCE obtained was 2.27% [31].

In this study, alkyl bithiophene and alkyl thienothiopehene were used as electron-donating units and DTBT moieties were used as the building blocks of an alternate copolymer to apply the band-gap-narrowing concept and thereby stabilize the HOMO level and obtain strong intermolecular π–π interaction. To compensate for the low solubility of DTBT, an alkoxy side chain was introduced into the benzothiadiazole core. The structure–property relationships caused by the difference between the bithiophene and fused thiophene donor molecules were investigated. To examine changes in the molecular energy level for different types of acceptor units, the acceptor units were compared using PQTPDTT, a polymer in which quinoxaline was used as an acceptor, by referring to previous studies. The synthesized DA-type polymers exhibited good crystallinity and low HOMO energy levels. In the synthesized polymer, PCE and V_{OC} were observed to increase to up to 3.9% and 0.878 V, respectively.

Experimental

Measurement and characterization

All reagents and chemicals were purchased from Aldrich and used as received unless otherwise specified. 4,7-Bis(5-bromothiophen-2-yl)-5,6-bis(octyloxy)-2,1,3-benzothiadiazole (A1) [43], 5,8-bis(5-bromothiophen-2-yl)-2,3-bis(4-(hexyloxy)phenyl)-6,7-bis(octyloxy)quinoxaline (A2), 4,4′-didodecyl-5-trimethylstannyl-2,2′-bithiophene (D1) [44], and 2,5-bis(trimethylstannyl)-3,6-dipentadecylthieno[3,2-b]thiophene (D2) [31] were prepared according to methods reported in the literature.

^{1}H NMR (400 MHz) spectra were recorded with a Bruker AMX400 spectrometer, using the resonances of the solvent as an internal reference. Chemical shifts (δ) are reported in ppm downfield from TMS. Absorption spectra were recorded on an Agilent 8453 UV–vis spectroscopy system. Photoluminescence (PL) spectra were measured using a Hitachi F-4500 spectrophotometer. The molecular weights of the polymers were measured using the GPC method with polystyrene standards. TGA measurements were performed on a TA Instruments 2050 analyzer. Electrochemical cyclic voltammetry was performed using a Zahner IM 6e electrochemical workstation with 0.1 M Bu_4NPF_6 in acetonitrile as the electrolyte. ITO glass coated with a thin polymer film was used as the working electrode, and a Pt wire and an Ag/Ag^+ electrode were used as the counter and reference electrodes, respectively. The electrochemical potential was calibrated against Fc/Fc^+. Current–voltage (I–V) curves of the PSC devices were measured using a computer-controlled Keithley 2400 source measurement unit (SMU) equipped with a Peccell solar simulator under AM1.5G illumination (100 mW cm^{-2}). The illumination intensity was calibrated using a standard Si photodiode detector equipped with a KG-5 filter. The output photocurrent was adjusted to match the photocurrent of the Si reference cell to obtain a power density of 100 mW cm^{-2}. The rated efficiency of 3.5% was measured with a P3HT/$PC_{61}BM$ reference cell under illumination and verified to be 3.4% under AM1.5G illumination (100 mW cm^{-2}) at Konkuk University (Korea). After encapsulation, all devices were operated under ambient atmospheric conditions at 25 °C.

Photovoltaic cell fabrication and treatment

All bulk heterojunction PV cells were prepared using the following device fabrication procedure. Glass/indium tin oxide (ITO) substrates [Sanyo, Japan (10 Ω/γ)] were sequentially patterned lithographically, cleaned with detergent, ultrasonicated in deionized water, acetone, and isopropyl alcohol, dried on a hot plate at 120 °C for 10 min, and treated with oxygen plasma for 10 min to improve the contact angle just before film coating. Poly(3,4-ethylene-dioxythiophene):poly(styrene-sulfonate) (PEDOT:PSS, Baytron P 4083 Bayer AG) was passed through a 0.45-mm filter before being deposited on ITO at a thickness of approximately 32 nm by spin-coating at 4000 rpm in air and then dried at 120 °C for 20 min inside a glove box. A blend of 1-(3-methoxycarbonyl)-propyl-1-phenyl-[6,6]-C71 ($PC_{71}BM$) and the polymer [1:2 (w/w), 1:3 (w/w), 1:4 (w/w)] at a concentration of 7.5 mg mL^{-1} in chlorobenzene was stirred overnight, filtered through a 0.2-mm poly(tetrafluoroethylene) (PTFE) filter, and then spin-coated (500–3000 rpm, 30 s) on top of the PEDOT:PSS layer. The device was completed by depositing thin layers of BaF_2 (1 nm) and Ba (2 nm) as an electron injection cathode, followed by the deposition of a 200-nm-thick aluminum layer at pressures below 10^{-6} torr. The active area of the device was 4 mm^2. Lastly, the cell was encapsulated using UV-curing glue (Nagase, Japan).

Hole-only devices were fabricated with a diode configuration of ITO(170 nm)/PEDOT:PSS (40 nm)/PQCQT:$PC_{71}BM$(50 nm)/MoO_3(30 nm)/Al(100 nm). The hole mobility of the active layers was calculated from the SCLC using the J–V curves of the hole-only devices measured in the dark as follows:

$$J = \frac{9}{8}\epsilon\epsilon_0\mu_{h(e)}\frac{V^2}{L^3}\exp\left(0.89\gamma\sqrt{\frac{V}{L}}\right)$$

where ε_0 is the permittivity of free space (8.85×10^{-14} F cm^{-1}); ε is the dielectric constant (assumed to be 3, which is a typical value for conjugated polymers) of the polymer; μ is the zero-field mobility of holes (electrons); L is the film thickness; and

($V = V_{appl} - V_r + V_{bi}$), where V_{appl} is the voltage applied to the device, V_r is the voltage drop due to the series resistance across the electrodes, and V_{bi} is the built-in voltage.

General procedure of polymerization through the Stille coupling reaction

In a 50-mL flame-dried flask, equimolar amounts (0.306 mmol) of A1 (or A2) and D1 (or D2) were dissolved in 18 mL of degassed toluene. Then, tris(dibenzylideneacetone)dipalladium(0) (Pd_2dba_3) (1.3 mol%) and tri-(*o*-tolyl)phosphine (6 mol%) were added as catalysts. The reaction mixture was vigorously stirred at 90–95 °C. After 48 h, 2-bromotihophene was added to the reaction, 3 h after which 2-trimethylstannyl thiophene was added and the reaction refluxed for 3 h to complete the end-capping reaction.

After cooling to room temperature, the polymer was poured into a methanol solution (300 mL) and filtered. The filtered polymer was further dissolved in $CHCl_3$ and reprecipitated into methanol and filtered. The polymer was further purified by washing in methanol, acetone and hexane, and $CHCl_3$, respectively, in a Soxhlet apparatus for 24 h. The chloroform fraction was recovered and dried under reduced pressure at 50 °C.

Poly[(3′,4″-didodecyl-2,2′:5′,2″:5″,2‴-quarterthiophene-alt-5, 6-bis(octyloxy) benzo[c][1,2,5]oxadiazole)], PABToBT

Black solid 0.14 g (yield = 47%). ^{1}H NMR ($CDCl_3$, ppm): δ 8.61 (m, 2*H*), 7.05 (m, 2*H*), 4.19 (s, 4*H*), 2.87 (s, 4*H*), 2.03 (s, 8*H*), 1.75 (s, 4*H*), 1.52 ~ 1.25 (m, 60*H*), 0.88 (m, 12*H*). Anal. Calcd. for $C_{62}H_{90}N_2O_2S_5$: C, 70.40; H, 8.77; N, 2.65; O, 3.03; S, 15.16. Found: C, 68.53; H, 9.00; N, 2.18; S, 13.78; O, 2.70.

Poly[3,6-dipentadecylthieno[3,2-b]thiophene-alt-5,6-bis(octyloxy)benzo[c][1,2,5] oxadiazole], PPDToBT

Black solid 0.17 g (yield = 51%). ^{1}H NMR ($CDCl_3$, ppm): δ 8.62 (m, 2*H*), 7.27 (m, 2*H*), 4.21 (s, 4*H*), 3.04 (s, 3*H*), 2.06 ~ 1.87 (m, 6*H*), 1.56 ~ 1.22 (m, 72*H*), 0.87 (m, 12*H*). Anal. Calcd. for $C_{66}H_{100}N_2O_2S_5$: C, 69.43; H, 8.35; N, 2.19; O, 2.50; S, 17.53. Found: C, 70.94; H, 8.77; N, 2.45; S, 15.06; O, 2.84.

Poly[2,3-bis(4-hexyloxyphenyl)quinoxaline-alt-2,5-bis(thieno-2-yl)-3,6-dipentade cyl thieno[3,2-b]thiophene], PQTPDTT

Dark red solid 0.3 g (yield = 63.7%). ^{1}H NMR ($CDCl_3$, ppm): δ 7.91(2*H*, br), 7.69 (2*H*, br), 7.6 (4*H*, br), 7.09 (2*H*, br), 6.88 (4*H*, br), 3.99 (4*H*, br), 3.0 (4*H*, br), 1.81 (8*H*, br), 1.56 (4*H*, br), 1.48 (4*H*, br), 1.35 (6*H*, br), 1.24 (40*H*, br), 0.92 (6*H*, br), 0.85 (6*H*, br). Anal. Calcd. for $C_{76}H_{102}N_2S_4O_2$: C, 75.84; H, 8.54; N, 2.33; S, 10.64; O, 2.66. Found: C, 75.14; H, 8.54; N, 2.20; S, 10.66; O, 2.68.

Results and discussion

Synthesis and characterization of the polymers

Scheme 1 outlines the chemical structures and synthesis process of the monomers and polymers. Both di-2-thienyl-2,1,3-benzothiadiazole (DTBT, A1) and di-2-thienyl-2,3-bis (4-hexyloxyphenyl)-5,8-dibromo quinoxaline (DTQ, A2) were used as acceptors, whereas 4,4′-didodecyl-5-trimethylstannyl-2,2′-bithiophene (biT, D1) and 2,5-bis (trimethylstannyl)-3,6-dipenta decylthieno[3,2-b]thiophene (TT, D2) were used as donors for the monomers and polymers.

To obtain good solubility in benzothiadiazole and quinoxaline derivatives (A1, A2), two octyloxy chains were introduced into the BT ring, and hexyloxy chains were introduced into the phenyl ring of the quinoxaline derivatives. A1, A2, D1, and D2 were synthesized using previously reported methods [31,44,45].

Using both acceptors (A1, A2) and donor derivatives (D1, D2), the following three polymers were obtained through a palladium-catalyzed Stille coupling reaction: poly[(5,5′-bis(thiophene-2-yl)-2,2′-(4,4′-didodecylbithiophene))-alt-(4,7-bis(5,6-bis(octyl oxy)-benzo[*c*][1,2,5]thiadiazole))] (PABToBT), poly[(5,5′-bis (thiophene-2-yl)-2,2′-(3,6-dipentadecynylthieno[3,2-b]thiophene))-alt-(4,7-bis(5,6-bis(octyloxy)benzo[*c*][1,2,5] thiadiazole))] (PPDToBT), and poly[2,3-bis(4-hexyloxyphenyl)quinoxaline-alt-2,5-bis (thieno-2-yl)-3,6-dipentadecylthieno[3,2-b]thiophene] (PQTPDTT).

The polymers obtained dissolved well in common organic solvents such as THF, chloroform, chlorobenzene, and *o*-dichlorobenze. The structures of the synthesized monomers and polymers were confirmed through ^{1}H NMR and EA (Experimental). Table 1 describes the molecular weight and thermal properties of the obtained polymers (PABToBT, PPDToBT, and PQTPDTT). As shown in this table, according to the GPC measurements performed using polystyrene as a standard, the number average molecular weights of PABToBT, PPDToBT, and PQTPDTT were 13,800, 38,200, and 34,700, respectively. The polydispersity indices (PDIs) were 1.47, 1.68, and 2.14, showing a very narrow distribution. The molecular weights of PPDToBT and PQTPDTT were high (M_n: 34–38 kg mol^{-1} or above, M_w: 62–74 kg/mol) because the solubility was improved by polymerization after a donor unit with a longer side chain was

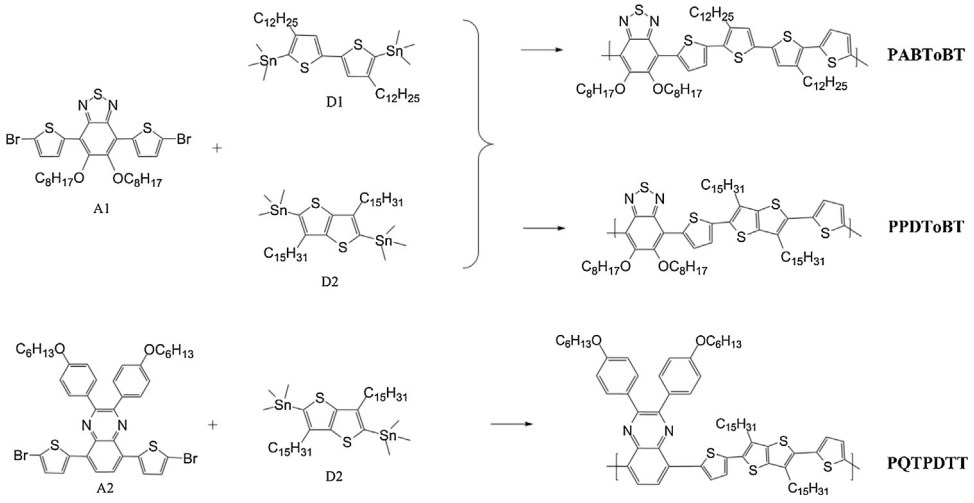

Scheme 1. Synthetic route for producing polymers.

Table 1
Physical and thermal properties of polymers.

Polymer	M_n [g/mol]	M_w [g/mol]	PDI	T_d [°C]
PABToBT	13800	20300	1.47	325
PPDToBT	38200	62300	1.63	331
PQTPDTT	34700	74500	2.14	347

Determined by GPC in tetrahydrofuran (THF) using polystyrene standards.

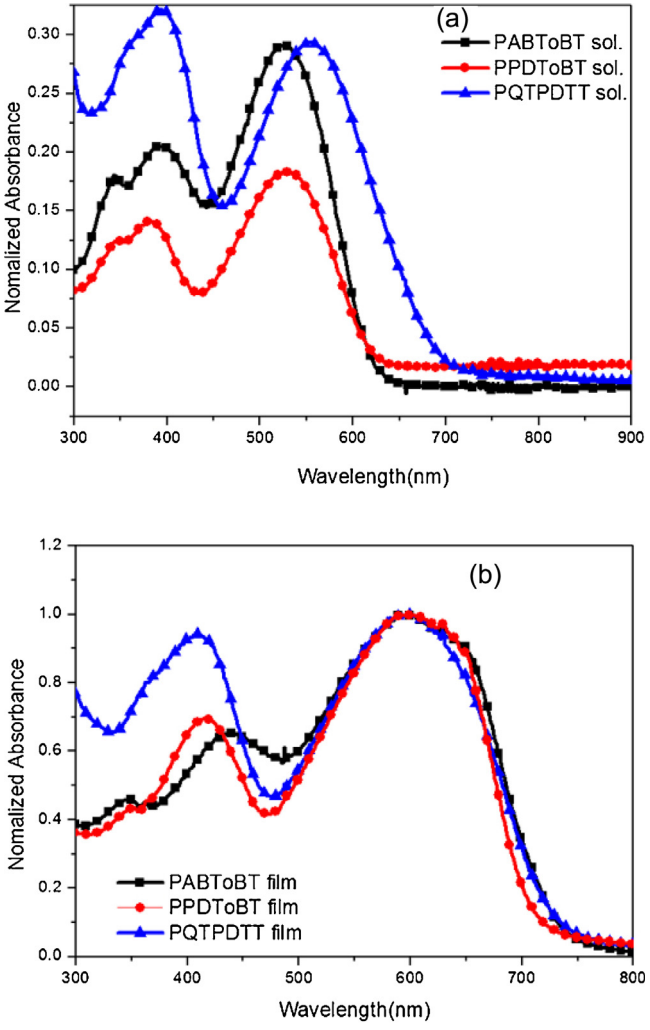

Fig. 1. UV–vis absorption spectra of polymers in solution (a) and film (b).

introduced [18,19]. But molecular weight of PABToBT wasn't high. It originated from a limitation of solubility. Solubility of monomer was good in toluene, but PABToBT precipitated after 12 h during polymerization.

Thermal stability

The thermal stability of the polymers was evaluated using TGA. According to the TGA measurements of PABToBT, PPDToBT, and PQTPDTT, 5% thermal weight loss in N_2 was observed at 325, 331, and 347 °C, respectively. Therefore, good thermal stability was observed for all polymers, confirming that they are suitable for device fabrication and application.

Optical properties

Fig. 1 shows the UV–vis spectra of PABToBT, PPDToBT, and PQTPDTT. Fig. 1(a) shows the absorption spectra of the solutions that formed when the polymers (PABToBT, PPDToBT, and PQTPDTT) were dissolved in $CHCl_3$ at a concentration of 10^{-5} M, whereas Fig. 1(b) shows the normalized absorption spectra obtained by drop-casting the polymer films onto a quartz substrate. Table 2 describes the optical data obtained, including the absorption peak wavelengths ($\lambda_{max,\ abs}$), absorption edge wavelengths ($\lambda_{edge,\ abs}$), and optical band gap ($E_{g,\ opt}$). All absorption spectra consisted of two absorption bands: a peak due to the localized π–π^* transition, which was observed at 300–450 nm, and a peak due to the intramolecular charge transfer (ICT) between the acceptor (BT, quinoxaline) and donor (thiophene derivatives) units, which was observed at 450–700 nm (long-wavelength region).

The maximum absorption peaks obtained when PABToBT, PPDToBT, and PQTPDTT were soluble were observed at 536, 527, and 544 nm, respectively. The molar absorption coefficients (ε) were 2.91×10^4, 1.83×10^4 M^{-1} cm^{-1}, and 3.21×10^4 M^{-1} cm^{-1}. When the molar absorption coefficient was compared among the three polymers, that of PQTPDTT was observed to be the highest, and it has been confirmed that the amount of photons absorbed could be increased further [45]. The absorption peaks (λ_{max}) in solid-state films of PABToBT, PPDToBT, and PQTPDTT were 596 nm, 569 nm, and 600 nm, respectively, representing red-shifts of 60, 59, and 40 nm relative to the liquid state.

The intermolecular interaction became stronger when the polymers were in the film state compared to that in the solution state. In addition, shoulder peaks were observed at 650, 600, and 640 nm, respectively, when PABToBT, PPDToBT, and PQTPDTT were in the film state due to strong π–π stacking among the polymeric backbones after the molecules formed a regular arrangement in the films. In PPDToBT and PQTPDTT, 2D-stacking was less effective compared to that in PABToBT because the coplanar thieno[3,2-b] thiophene unit was twisted with the spacer, and a tilting angle between the donor moiety and thiophene spacer was relatively large. As a result, the UV–vis peaks of PPDToBT and PQTPDTT were less red-shifted in the solid state [46].

The optical band gaps of PABToBT, PPDToBT, and PQTPDTT from the UV–vis absorption edge on the film were 1.70, 1.75, and 1.71 eV, respectively. In the films, the UV–vis peaks of the polymers were red-shifted relative to those in the UV–vis spectrum

Table 2
Optical and electrochemical data of all polymers.

Polymer	UV–vis absorption				Cyclic voltammetry	
	$CHCl_3$ solution		Film			
	λ_{max} [nm]	λ_{max} [nm]	λ_{onset} [nm]	E_g^{opt} [a] [eV]	E_{onset}^{ox} (V)/HOMO [eV]	LUMO [b] [eV]
PABToBT	400, 536	440, 596	728	1.70	0.69/−5.04	−3.34
PPDToBT	388, 538	405, 597	709	1.75	0.94/−5.27	−3.52
PQTPDTT	393, 554	409, 594	723	1.71	0.90/−5.25	−3.55

[a] Calculated from the intersection of the tangent on the low energetic edge of the absorption spectrum with the baseline.
[b] LUMO = HOMO + E_g.

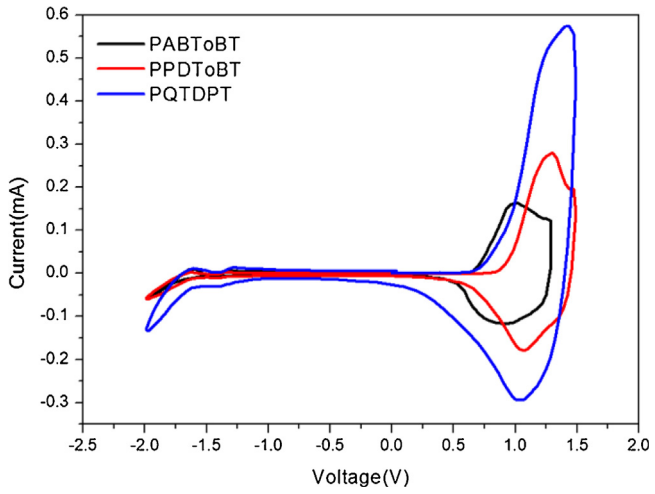

Fig. 2. Cyclic voltammograms of polymers.

of P3HT (absorption edge at −650 nm) because of the introduction of benzothiadiazole and quinoxaline derivatives, which increased the optical absorption domain with electron-withdrawing properties [32]. The same acceptor unit (A1) was introduced into PABToBT and PPDToBT. Due to the difference in the tilt angle between the donor moiety and spacer, however, the conjugation length was shortened in PPDToBT, which was accompanied by a decline in stacking properties. As a result, the band gap was further widened. Even though the same donor unit (D2) was introduced into PPDToBT and PQTPDTT, the band gap of PQTPDTT was smaller than that of PPDToBT because the quinoxaline derivatives (acceptor moiety) had a lower LUMO energy level and greater electron-withdrawing characteristics than BT.

Electrochemical properties

The electrochemical properties of the three polymers were measuring by cyclic voltammetry (CV). The film that was formed by drop-casting the polymer dissolved in $CHCl_3$ on an ITO glass electrode was used as a working electrode. The electrode was measured in a N_2 atmosphere with 0.1 M Bu_4NPF_6 in acetonitrile as the electrolyte. The CV results are shown in Fig. 2 and summarized in Table 2.

The HOMO levels were calculated based on the oxidation potential measured through CV. The HOMO energy levels estimated from the electrochemical oxidation onsets (0.69 V, 0.94 V, 0.90 V) for PABToBT, PPDToBT, and PQTPDTT were −5.04 eV, −5.27 eV and −5.25 eV, respectively. These results are in agreement with the conclusion that the HOMO energy level is primarily determined by a donor unit in the case of a donor–acceptor copolymer. That is, because the HOMO energy level of the alkyl thieno[3,2-b]thiophene electron-donating unit of PPDToBT and PQTPDTT is relatively lower than the alkyl bithiophene electron-donating unit of PABToBT, the HOMO energy level of PPDToBT and PQTPDTT is deeper than that of PABToBT [47]. The HOMO energy levels of both PPDToBT and PQTPDTT were deeper than the HOMO level of PABToBT by −0.21 to −0.23 eV. This result is similar to that obtained for the HOMO energy level of alkyl thieno[3,2-b]thiophene, which was lower than that of alkyl bithiophene by approximately −0.3 eV according to density functional theory (DFT) calculations. In addition, the alkyl side chain introduced into the fused thiophene units was pentadecyl, which was longer than the dodecyl moiety introduced into the bithiophene units, in agreement with the result indicating that the side chain gave rise to a lower HOMO level [18,19].

It has been verified that the difference in the HOMO levels between the PPDToBT and PQTPDTT containing the same TT donor units is not dependent on the donor unit only. Because the BT introduced as an acceptor unit had a lower HOMO level than the

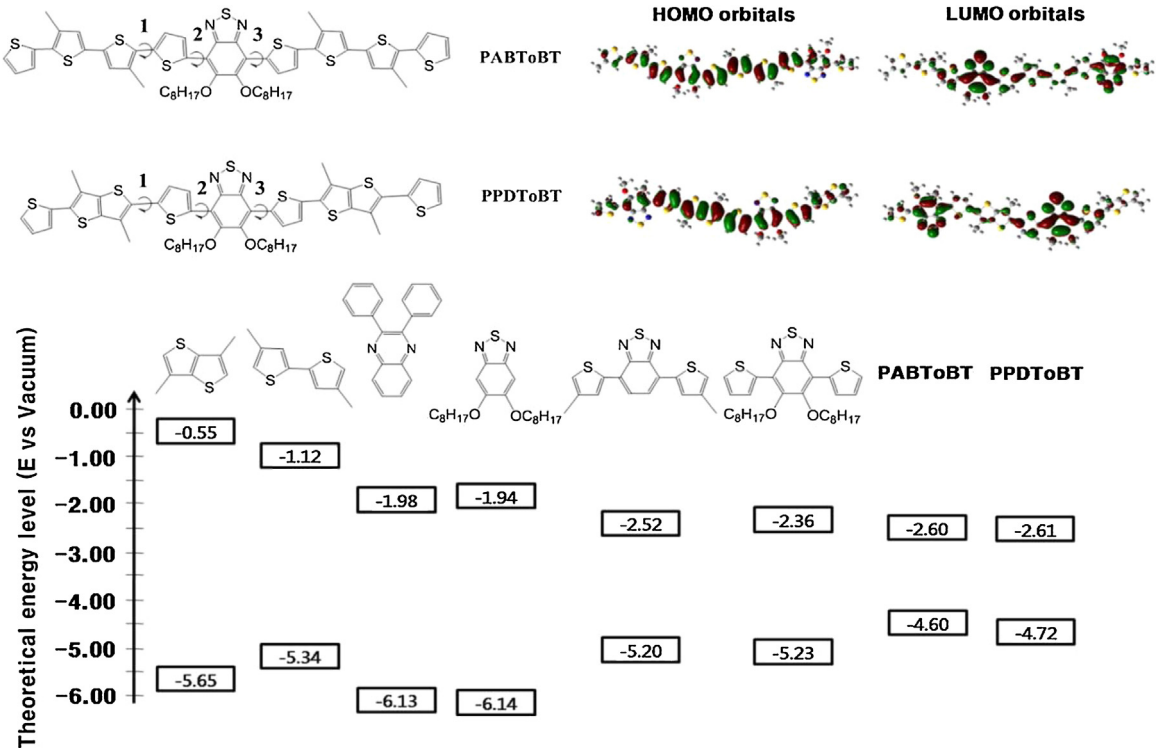

Fig. 3. The calculated LUMO and HOMO orbitals for monomer units and the dimer models of polymers.

quinoxaline derivatives, PPDToBT also exhibited a lower HOMO level (approximately −5.30 eV) than PQTPDTT. This result is in agreement with that obtained by W. You regarding the HOMO level of a polymer containing BT, which has a side chain in the core [48]. Because PPDToBT has the deepest-lying HOMO level, it appears that, theoretically, it would have a high open-circuit voltage (V_{OC}) [47].

The LUMO levels calculated based on the differences in the HOMO energy levels and optical band gap energies of PABToBT, PPDToBT, and PQTPDTT were −3.34 eV, −3.52, and −3.55 eV, respectively. The LUMO energy levels of the three polymers are within a reasonable range. In addition, the LUMO energy levels are far greater than those of $PC_{61}BM$ and $PC_{71}BM$ (approximately −3.7 to −4.1 eV).

The difference in the LUMO energy levels between PPDToBT and PQTPDTT is due to the differences in the electron affinities of the electron-deficient units introduced into the molecular structure. Because quinoxaline derivatives have a stronger electron affinity than BT, the ICT effect was activated. As a result, the LUMO level decreased [49].

To understand the electronic properties of the synthesized polymers, the molecular geometries and distribution of the electron density of states were simulated using DFT calculations based on a hybrid B3LYP-correlation functional and a split valence 6–31G(d) basis set. The calculations were performed using Gaussian 09. Oligomers with two repeat units were chosen for the calculation model.

Fig. 3 shows the HOMO and LUMO orbitals calculated using the repeating unit models. The structure used as a model was calculated by simplifying a side chain with methyl. The HOMO orbitals are delocalized on the polymer main chain, whereas the LUMO orbitals are localized on the quinoxaline and BT (acceptor) derivatives because of the structural characteristics that form a quinoid, an unshared electron pair of nitrogen, and the electron-withdrawing properties of sulfur [50,51].

Based on the cyclic voltammetry measurements, PPDToBT and PQTPDTT exhibited lower HOMO levels than PABToBT (−4.72 eV). The quinoxaline acceptor exhibited slightly higher HOMO levels and lower LUMO levels than BT.

The dihedral angles between two thienyl groups with a central BT and bithiophene/thienothiophene were measured as shown in Fig. 3; the results are summarized in Table 3.

The dihedral angles of PABToBT and PPDToBT were 13° and 30°, respectively. The dihedral angle of fused thiophene was nearly double that of bithiophene because the rigid and coplanar fused thiophene is less flexible than bithiophene.

X-ray diffraction patterns

To analyze the crystal structure of the thin films of PABToBT and PPDToBT, the X-ray diffraction patterns of the polymer films formed on a silicon wafer were measured (Fig. 4(a)). Out-of-plane mode measurements indicated sharp (h00) diffraction peaks at $2\theta = 3.88°$ and 7.64° for PABToBT and at $2\theta = 3.96°$ and 7.96° for PPDToBT. The (h 0 0) peak measured out of plane corresponds to the formation and conventional edge-on π-stacking of an ordered lamellar structure by the alkyl side chains of the bithiophene and thienothiopehene donor units [46]. The lamellar d-spacings (d_1) of PABToBT and PPDToBT were calculated to be 22.77 and 22.31 Å ($\lambda = 2d[\sin\theta]$), respectively.

The (0 h 0) peak associated with the π–π stacking distance is shown in the inset of Fig. 4. Broad diffraction peaks were observed at $2\theta = 22.30°$ and $2\theta = 24.06°$ for PABToBT and PPDToBT, respectively. The π–π stacking distances (d_π) calculated using the same formula were 3.99 and 3.62 Å, respectively, indicating that the π–π stacking was more effective in PPDToBT than in PABToBT.

XRD measurements were performed for the blended films to confirm structural ordering in blended films (Fig. 4(b)). In the out-of-plane of polymer: $PC_{70}BM$ blend film, a stronger (0 1 0) diffraction peak was prominently detected at 18.5 and, 18.8° which originates from crystalline of fullerenes. The addition of $PC_{71}BM$ into PABToBT and PPDToBT generated the (0 1 0) peak with the higher order of π–π stacking. The interlamellar spacing for PPDToBT:$PC_{71}B$ increased from 3.62 to 4.72 Å, which is indicating that $PC_{71}BM$ was interdigitated between polymer chains bicontinuous and tightly[52]. The interlamellar spacing for PABToBT:$PC_{71}BM$ also increased from 3.99 to 4.80 Å.

PPDToBT show shorter d_π-spacing both polymer and blend film states. These results are similar to those observed for benzene–thiophene aromatic system polymers that have exhibited good performance in OPVs [50]. Thus, 2θ values with relatively high-intensity (h 0 0) and (0 h 0) peaks compared to those of PABToBT were observed for PPDToBT. That is, the intermolecular distances

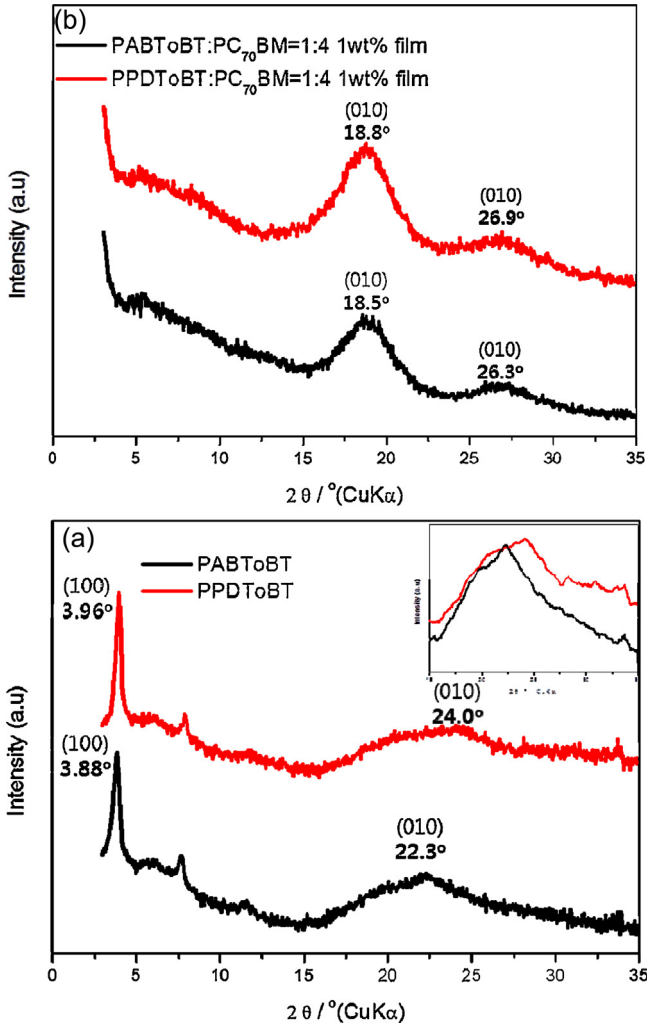

Fig. 4. Out-of-plane X-ray diffraction patterns of PABToBT and PPDToBT films (a), polymer:$PC_{71}BM$ blend films (b) on silicon wafers.

Table 3
Calculated parameters.

Polymer	Dihedral angle (deg)			$HOMO^{cal}$ [eV]	$LUMO^{cal}$ [eV]
	1	2	3		
PABToBT	13	14–15	14–15	−4.60	−2.60
PPDToBT	30	14–15	14–15	−4.72	−2.61

(d_1, d_π) were close. It appears that these characteristics result in a high J_{SC} in the fabrication of a BHJ SC by greatly enhancing the charge transport of PPDToBT [34].

PPDToBT showed a greater tilt angle than PABToBT. However, effective π–π stacking occurred in PPDToBT because the fused thiophene ring (tilt angle: 0°) exhibits strong planarity between the chain backbones. As shown in the XRD measurements in Fig. 4, PPDToBT exhibited a shorter π–π stacking distance than PABToBT. It appears that a high FF would occur in OPVs due to the close π–π stacking of PPDToBT.

Photovoltaic properties

Fig. 5(a)–(c) show the *J*–*V* curves of photovoltaic devices fabricated using PABToBT, PPDToBT, and PQTPDTT, respectively, and Fig. 5(d)–(f) show their IPCE spectra. The photovoltaic properties of the two polymers were evaluated by fabricating PSC devices with an ITO/PEDOT:PSS/polymer:$PC_{71}BM$/Ba/BaF_2/Al structure. The results are summarized in Table 4 and Fig. 6.

All of the polymers exhibited the best performance under 100 mW cm^{-2} AM1.5G illumination when the polymer:$PC_{71}BM$ ratio was 1:4 (w/w %). The device containing a blend of PABToBT and $PC_{71}BM$ in a 1:4 ratio had an open-circuit voltage (V_{OC}) of 0.838 V, a short-circuit current (J_{SC}) of 8.7 mA cm^{-2}, a fill factor (FF) of 51.5%, and a power conversion efficiency (PCE) of 3.8%.

For the device containing a blend of PPDToBT and $PC_{71}BM$ in a 1:4 ratio, the V_{OC}, J_{SC}, FF, and PCE were measured to be 0.878 V, 8.7 mA cm^{-2}, 50.7%, and 3.9%, and for the device containing a blend of PQTPDTT and $PC_{71}BM$ in a 1:4 ratio, the values were determined to be 0.878 V, 7.0 mA cm^{-2}, 39.8%, and 2.4%, respectively.

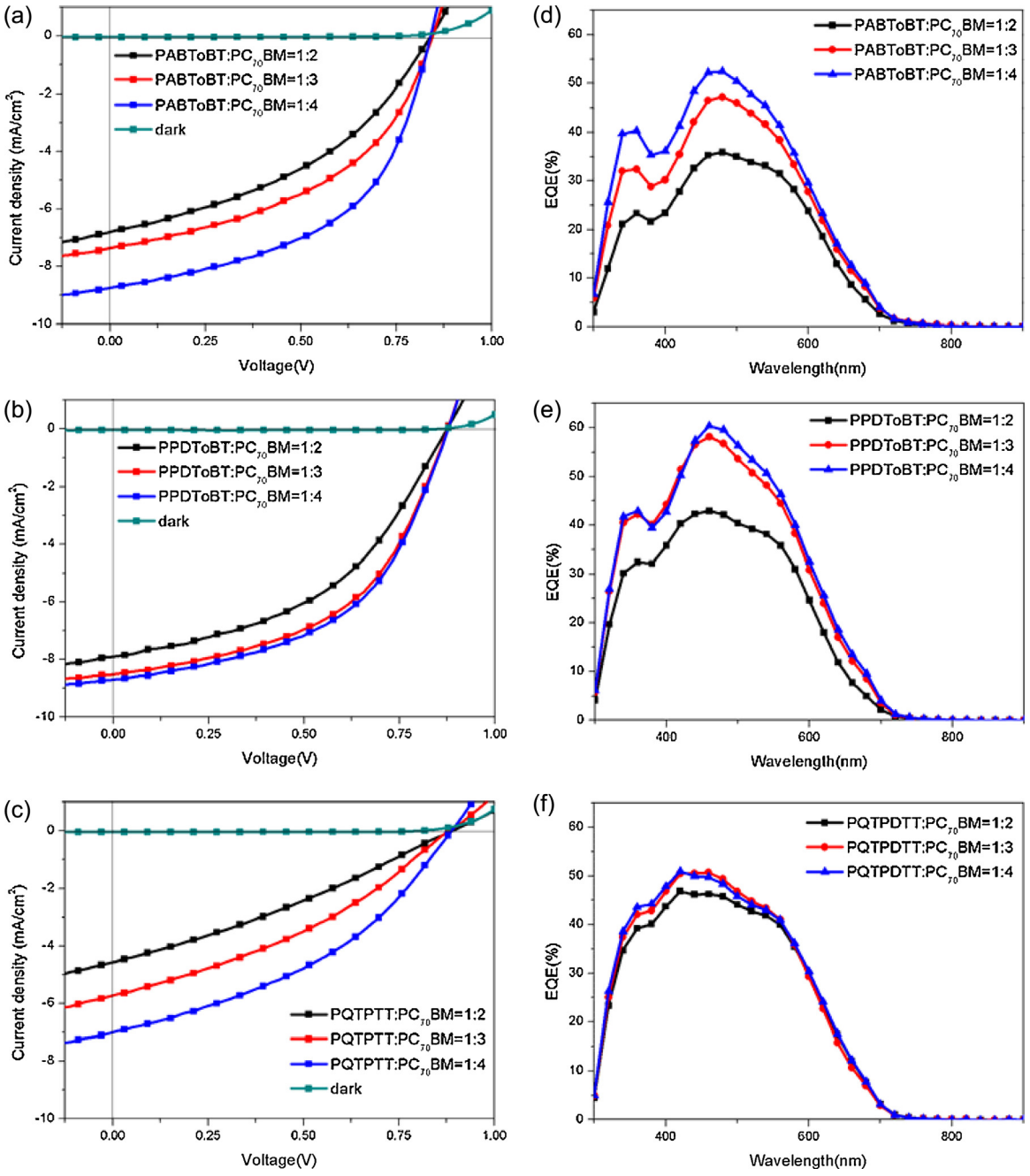

Fig. 5. (a)–(c) *J*–*V* curves of PSCs with different polymer:$PC_{71}BM$ ratios under AM1.5G illumination, 100 mW/cm^2. (d)–(f) The IPCE spectra of PSCs with different polymer:$PC_{71}BM$ ratios.

Table 4
Photovoltaic properties of polymers.

Polymer	$PC_{71}BM$ Ratios (w:w)	V_{OC} [V]	J_{SC} [mA/cm^2]	FF [%]	PCE [%]	IPCE [%/nm]	R_S (Ω cm^2)	R_{SH} (Ω cm^2)
PABToBT	1: 2	0.838	6.8	41	2.3	35.9/480	49.5	351
	1: 3	0.838	7.3	46.3	2.8	47.2/480	28.6	556
	1: 4	0.838	8.7	51.5	3.8	52.4/480	19.1	627
PPDToBT	1: 2	0.878	7.9	45.0	3.1	42.9/460	43.5	625
	1: 3	0.878	8.5	50.1	3.7	58.1/460	27.2	713
	1: 4	0.878	8.7	50.7	3.9	60.4/460	26.4	914
PQTPDTT	1: 2	0.878	4.5	30.6	1.2	46.8/420	171	291
	1: 3	0.878	5.7	34.9	1.7	50.7/460	112	306
	1: 4	0.878	7.0	39.8	2.4	50.9/420	57.8	312

The V_{OC} of the devices fabricated with polymer:$PC_{71}BM$ blends of PABToBT, PPDToBT, and PQTPDTT were 0.838 V, 0.878 V, 0.878 V, respectively. It was expected that PPDToBT would have the highest V_{OC} due to its deeper-lying HOMO level [47]. As shown in Table 4, PPDToBT and PQTPDTT exhibited higher V_{OC} values than PABToBT in the devices fabricated with various PCBM ratios. With each polymer, as the PCBM ratio increased, both J_{SC} and FF tended to increase. This behavior can be explained by considering the series resistance (R_S) and shunt resistance (R_{SH}). As the PCBM ratio increases, R_S decreases, whereas R_{SH} increases, which results in a decrease in the probability of an exciton being recombined and in the improvement of the interfacial characteristics with a buffer layer [46].

These devices revealed a broad EQE graph within the visible range. A large EQE was detected at 300–700 nm, but at 700 nm or above, the EQE was low. In the PPDToBT blend-based devices, a high EQE (up to 60.4%) was observed at 460 nm, which matches the high photocurrent value. The J_{SC} values of PABToBT and PQTPDTT were lower than that of PPDToBT, even though the molar absorption coefficients of PABToBT and PQTPDTT were higher than that of PPDToBT because of a high R_S and low EQE.

Thin-film morphology and charge-carrier mobility

In BHJ solar cells, the hole mobility in the polymer layer is extremely important to the photovoltaic performance. We used a space charge limited current (SCLC) model, which is based on the Poole–Frenkel law, to determine the hole mobility in blends containing $PC_{71}BM$. The typical result is plotted as $\ln(JL^3/V^2)$ vs $(V/L)^{1/2}$, as shown in ESI*. Herein, J refers to current density, d refers to the thickness of the device, and $V = V_{appl} - V_{bi}$, where V_{appl} is the applied potential and V_{bi} is the built-in potential [53]. Hole-only devices were fabricated with a diode configuration of ITO(170 nm)/PEDOT:PSS(40 nm)/polymer:$PC_{71}BM$/MoO_3(30 nm)/Al(100 nm).

According to the equation $V = V_{appl} - V_{bi}$ and Figs. S4–S6, which plot $\ln(Jd^3/V^2)$ vs $(V/d)^{1/2}$, the hole mobility of the three polymers blended with $PC_{71}BM$ (1:4 ratio) are quite different: 3.27×10^{-3} cm^2 V^{-1} s^{-1}, 3.21×10^{-2} cm^2 V^{-1} s^{-1}, and 3.46×10^{-4} cm^2 V^{-1} s^{-1}(Figs. S5–S7 in theSupporting information). The results show that the PPDToBT/PCBM blend device obtained a high mobility, which may have been due to the larger planar structure and close π–π stacking of the copolymer.

In addition to absorbance and energy level, the surface morphology of polymer blends is a critical factor in determining the efficiency of PSCs. Therefore, the morphologies of the polymer/PCBM blend films were verified by AFM (Fig. S8). In general, the surfaces of the PPDToBT and $PC_{71}BM$ blended films were smooth. In contrast, the PABToBT blend film showed black dots with a highly aggregated PCBM domain. At 1:2 (w/w %) in particular, the greatest extent of phase separation and the roughest surface with a root-mean-square (RMS) roughness of 0.398 nm were detected.

As the PCBM ratio increased from 1:2 to 1:4, the RMS roughness tended to decrease. Both J_{SC} and FF were high for the three polymers when the polymer:$PC_{71}BM$ ratio was 1:4 (w/w %) through the optimization of the blend morphologies. At this ratio, the PABToBT, PPDToBT, and PQTPDTT blended films had RMS roughnesses of 0.330 nm, 0.233 nm, and 0.409 nm, respectively. Thus, the best morphology was observed in the PPDToBT-blended film. As the roughness of the film increased, the FF declined. In addition, electron/hole conduction was limited and the charge carriers experienced recombination, which caused a decrease in J_{SC} and hole mobility.

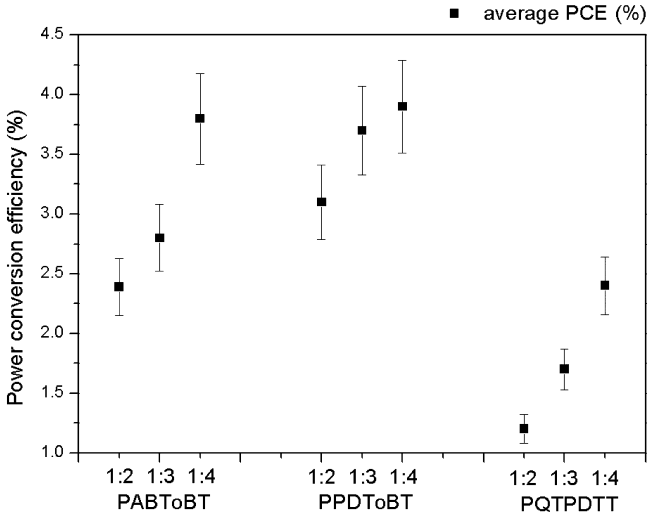

Fig. 6. Average values and error bars of PSCs with different polymer:$PC_{71}BM$ ratios under AM1.5G illumination, 100 mW/cm^2.

Conclusions

In this study, conjugated polymers-PABToBT, PPDToBT, and PQTPDTT-were obtained by introducing thiophene-based donor moieties and benzothiadiazole/quinoxaline as acceptor units through the Stille coupling reaction. All three polymers exhibited superior crystallinity and thermal stability and low HOMO levels. It was verified that the energy levels of CT-type polymers are affected by the energy levels of both the acceptor and the donor. These desirable properties offer advantages in applicability to solar cells. When the polymer:$PC_{71}BM$ ratio was 1:4 (w/w %), PABToBT showed J_{SC}, V_{OC}, FF, and PCE values of 8.7 mA cm^{-2}, 0.834 V, 51.5%, and 3.8%, whereas PPDToBT showed values of 8.7 mA cm^{-2}, 0.878 V, 50.7%, and 3.9%, respectively, demonstrating the best performance.

Competing interest

The authors declare no competing financial interest.

Acknowledgements

This research was supported by the National Research Foundation of Korea Grant funded by the Korean Government (MEST) (NRF-2012M1A2A2671703).

Appendix A. Supplementary data

Supplementary data associated with this article can be found, in the online version, at doi:10.1016/j.jiec.2014.10.045.

References

[1] J. Wang, C.-q. Zhang, C.-m. Zhong, S.-j. Hu, X.-y. Chang, Y.-q. Mo, X. Chen, H.-b. Wu, Macromolecules 44 (2010) 17.
[2] J.Y. Lee, M.H. Choi, D.K. Moon, J.R. Haw, J. Ind. Eng. Chem. 16 (2010) 395.
[3] A. Najari, S. Beaupré, P. Berrouard, Y. Zou, J.-R. Pouliot, C. Lepage-Pérusse, M. Leclerc, Adv. Funct. Mater. 21 (2011) 718.
[4] S. Changsarn, J.D. Mendez, C. Weder, P. Supaphol, Macromol. Mater. Eng. 293 (2008) 952.
[5] Y. Li, P. Sonar, S.P. Singh, M.S. Soh, M. van Meurs, J. Tan, J. Am. Chem. Soc. 133 (2011) 2198.
[6] P.M. Beaujuge, W. Pisula, H.N. Tsao, S. Ellinger, K. Mu?llen, J.R. Reynolds, J. Am. Chem. Soc. 131 (2009) 7514.
[7] J. Fanous, M. Schweizer, D. Schawaller, M.R. Buchmeiser, Macromol. Mater. Eng. 297 (2012) 123.
[8] H. Bronstein, Z. Chen, R.S. Ashraf, W. Zhang, J. Du, J.R. Durrant, P. Shakya Tuladhar, K. Song, S.E. Watkins, Y. Geerts, M.M. Wienk, R.A.J. Janssen, T. Anthopoulos, H. Sirringhaus, M. Heeney, I. McCulloch, J. Am. Chem. Soc. 133 (2011) 3272.
[9] G. Zhao, Y. He, C. He, H. Fan, Y. Zhao, Y. Li, Sol. Energy Mater. Sol. Cells 95 (2011) 704.
[10] L. Huo, J. Hou, S. Zhang, H.-Y. Chen, Y. Yang, Angew. Chem. Int. Ed. 49 (2010) 1500.
[11] R.S. Ashraf, J. Gilot, R.A.J. Janssen, Sol. Energy Mater. Sol. Cells 94 (2010) 1759.
[12] S.W. Heo, K.H. Baek, H.J. Song, T.H. Lee, D.K. Moon, Macromol. Mater. Eng. 299 (2014) 353.
[13] F.C. Krebs, T. Tromholt, M. Jorgensen, Nanoscale 2 (2010) 873.
[14] F.C. Krebs, J. Fyenbo, M. Jorgensen, J. Mater. Chem. 20 (2010) 8994.
[15] R.R. Søndergaard, M. Hösel, F.C. Krebs, J. Polym. Sci., B: Polym. Phys. 51 (2013) 16.
[16] R.P. Singh, O.S. Kushwaha, Macromol. Symp. 327 (2013) 128.
[17] G. Li, V. Shrotriya, J. Huang, Y. Yao, T. Moriarty, K. Emery, Y. Yang, Nat. Mater. 4 (2005) 864.
[18] J.Y. Lee, M.H. Choi, H.J. Song, D.K. Moon, J. Polym. Sci., A: Polym. Chem. 48 (2010) 4875.
[19] J.Y. Lee, M.H. Choi, S.W. Heo, D.K. Moon, Synth. Met. 161 (2011) 1.
[20] J. Peet, J.Y. Kim, N.E. Coates, W.L. Ma, D. Moses, A.J. Heeger, G.C. Bazan, Nat. Mater. 6 (2007) 497.
[21] E. Wang, L. Wang, L. Lan, C. Luo, W. Zhuang, J. Peng, Y. Cao, Appl. Phys. Lett. 92 (2008) 033307.
[22] E. Zhou, S. Yamakawa, K. Tajima, C. Yang, K. Hashimoto, Chem. Mater. 21 (2009) 4055.
[23] R. Qin, W. Li, C. Li, C. Du, C. Veit, H.-F. Schleiermacher, M. Andersson, Z. Bo, Z. Liu, O. Inganäs, U. Wuerfel, F. Zhang, J. Am. Chem. Soc. 131 (2009) 14612.
[24] C.-P. Chen, S.-H. Chan, T.-C. Chao, C. Ting, B.-T. Ko, J. Am. Chem. Soc. 130 (2008) 12828.
[25] A. Gadisa, W. Mammo, L.M. Andersson, S. Admassie, F. Zhang, M.R. Andersson, O. Inganäs, Adv. Funct. Mater. 17 (2007) 3836.
[26] F.C. Krebs, N. Espinosa, M. Hösel, R.R. Søndergaard, M. Jørgensen, Adv. Mater. 26 (2014) 29.
[27] J.-Y. Lee, S.-H. Kim, I.-S. Song, D.-K. Moon, J. Mater. Chem. 21 (2011) 16480.
[28] L. Biniek, C.L. Chochos, G. Hadziioannou, N. Leclerc, P. Lévêque, T. Heiser, Macromol. Rapid Commun. 31 (2010) 651.
[29] F. Liang, J. Lu, J. Ding, R. Movileanu, Y. Tao, Macromolecules 42 (2009) 6107.
[30] W. Yue, Y. Zhao, H. Tian, D. Song, Z. Xie, D. Yan, Y. Geng, F. Wang, Macromolecules 42 (2009) 6510.
[31] J.-Y. Lee, W.-S. Shin, J.-R. Haw, D.-K. Moon, J. Mater. Chem. 19 (2009) 4938.
[32] P. Vemulamada, G. Hao, T. Kietzke, A. Sellinger, Org. Electron. 9 (2008) 661.
[33] I. McCulloch, M. Heeney, C. Bailey, K. Genevicius, I. MacDonald, M. Shkunov, D. Sparrowe, S. Tierney, R. Wagner, W. Zhang, M.L. Chabinyc, R.J. Kline, M.D. McGehee, M.F. Toney, Nat. Mater. 5 (2006) 328.
[34] L. Biniek, S. Fall, C.L. Chochos, D.V. Anokhin, D.A. Ivanov, N. Leclerc, P. Léve?que, T. Heiser, Macromolecules 43 (2010) 9779.
[35] H. Zhou, L. Yang, S. Xiao, S. Liu, W. You, Macromolecules 43 (2010) 811.
[36] H. Zhou, L. Yang, S.C. Price, K.J. Knight, W. You, Angew. Chem. Int. Ed. 49 (2010) 7992.
[37] X. Wang, Y. Sun, S. Chen, X. Guo, M. Zhang, X. Li, Y. Li, H. Wang, Macromolecules 45 (2012) 1208.
[38] P.M. Oberhumer, Y.-S. Huang, S. Massip, D.T. James, G. Tu, S. Albert-Seifried, D. Beljonne, J. Cornil, J.-S. Kim, W.T.S. Huck, N.C. Greenham, J.M. Hodgkiss, R.H. Friend, J. Chem. Phys. 134 (2011) 114901.
[39] W. Li, R. Qin, Y. Zhou, M. Andersson, F. Li, C. Zhang, B. Li, Z. Liu, Z. Bo, F. Zhang, Polymer 51 (2010) 3031.
[40] C. Du, C. Li, W. Li, X. Chen, Z. Bo, C. Veit, Z. Ma, U. Wuerfel, H. Zhu, W. Hu, F. Zhang, Macromolecules 44 (2011) 7617.
[41] G. Tu, S. Massip, P.M. Oberhumer, X. He, R.H. Friend, N.C. Greenham, W.T.S. Huck, J. Mater. Chem. 20 (2010) 9231.
[42] S. Song, Y. Jin, S.H. Kim, J. Moon, K. Kim, J.Y. Kim, S.H. Park, K. Lee, H. Suh, Macromolecules 41 (2008) 7296.
[43] M. Helgesen, S.A. Gevorgyan, F.C. Krebs, R.A.J. Janssen, Chem. Mater. 21 (2009) 4669.
[44] H. Usta, C. Risko, Z. Wang, H. Huang, M.K. Deliomeroglu, A. Zhukhovitskiy, A. Facchetti, T.J. Marks, J. Am. Chem. Soc. 131 (2009) 5586.
[45] J.Y. Lee, K.W. Song, J.R. Ku, T.H. Sung, D.K. Moon, Sol. Energy Mater. Sol. Cells 95 (2011) 3377.
[46] H.J. Song, T.H. Lee, M.H. Han, J.Y. Lee, D.K. Moon, Polymer 54 (2013) 1072.
[47] Q. Zheng, B.J. Jung, J. Sun, H.E. Katz, J. Am. Chem. Soc. 132 (2010) 5394.
[48] H. Zhou, L. Yang, S. Xiao, S. Liu, W. You, Macromolecules 43 (2009) 811.
[49] H. Zhou, L. Yang, S. Stoneking, W. You, ACS Appl. Mater. Interfaces 2 (2010) 1377.
[50] H.-J. Song, D.-H. Kim, E.-J. Lee, S.-W. Heo, J.-Y. Lee, D.-K. Moon, Macromolecules 45 (2012) 7815.
[51] H.-J. Song, D.-H. Kim, E.-J. Lee, D.-K. Moon, J. Mater. Chem. A 1 (2013) 6010.
[52] W. Lee, G.-H. Kim, S.-J. Ko, S. Yum, S. Hwang, S. Cho, Y.-H. Shin, J.Y. Kim, H.Y. Woo, Macromolecules 47 (2014) 1604.
[53] L. Xiao, J. Yuan, Y. Zou, B. Liu, J. Jiang, Y. Wang, L. Jiang, Y.f. Li, Synth. Met. 187 (2014) 201.